Automation of the Bird Shoulder Joint Deboning

Debao Zhou, Jonathan Holmes, Wiley Holcombe and Gary McMurray

Food Processing Technology Division, ATAS Laboratory, Georgia Tech Research Institute (GTRI),
Georgia Institute of Technology, Atlanta, GA 30332-0823

Abstract—**Poultry deboning processing is one of the largest employers of people in the United States. It involves mainly manual processes with only limited use of fixed automation. The main difficulty in this task is the unstructured nature of the task due to the natural variability of birds' size and deformable bodies. To increase product safety and quality, the industry is looking to robotics to help solve these problems. This research has focused on automating cutting of bird front halves. The anatomic structure of the chicken shoulder joint was studied first. Thus the cutting locations on chicken front halves were identified. In conjunction with force control robotics, a 3-DOF device with the capability for size adaptation and deformation compensation was proposed and the cutting trajectory was simulated. The results of the dynamic simulation verified that the desired trajectory can be followed and the response time for bone detection can be satisfied. A functional prototype of this device has been built and is currently under evaluation.**

***Index Terms*—Front half, anatomy, deboning, robotic device.**

I. Introduction

Figure 1 (a) shows a bird with a marked front half. Figure 1 (b) shows the procedure to manually harvest butterflies, as shown in Figure 1(d), from front halves in a poultry plant. A front half is first cut away from a bird and then it is put on a cone for deboning. After the joint connections are severed, the wing and breast meat are separated from the carcass as shown in Figure 1(c) by generating a relative motion between the wings and the carcass.

Considering this process has to be manually repeated on approximately 300,000 of chickens each day, it is obviously very onerous. However, due to the naturally deformable bodies, size difference and possible hard bone chips in meat, its automation is very challenging. One commercial solution is from the automation deboning lines from the Stork Gamco Inc. [1]. However, their method still belongs to the fixed automation category since they require the cutting motions be preset manually and thus, they cannot automatically adjust to changes in individual bird sizes. Meyn Inc. [2] also developed a cutting device. Their cutting device has only one fixed motion for all the front halves deboning. In order to adapt to variations in the chicken size, Daley *et al*. [3] proposed a reference-point method to estimate the locations of the cutting trajectory. The reference points were obtained through the analysis of the computer images. Using a similar method, Heck [4] proposed to use a water-jet cutting method to cut chicken breast meat to obtain certain shapes according to the identified trajectory from computer images. Beyond chicken, some research on deboning has been carried out on the pork or beef such as [5] and [6]. Their pork and beef deboning method is to cut through everything including hard bones, while the chicken deboning try to avoid hard bones in order to obtain high quality butterflies.

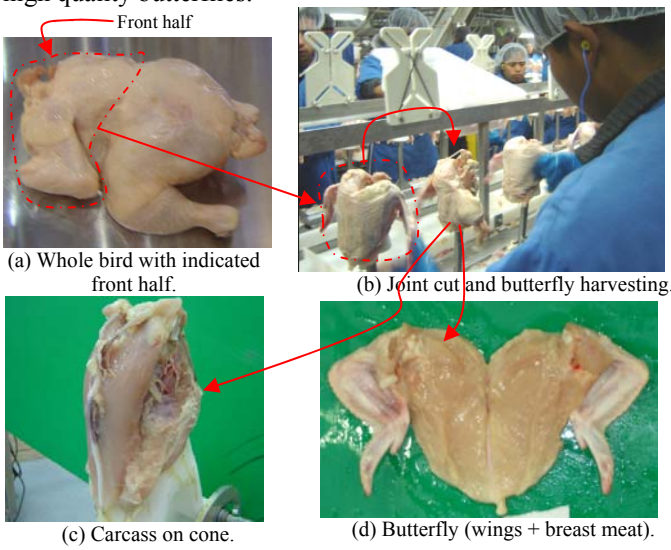

(a) Whole bird with indicated front half. (b) Joint cut and butterfly harvesting. (c) Carcass on cone. (d) Butterfly (wings + breast meat).

Figure 1: Illustration of the harvesting of chicken butterfly.

Currently, no cutting device is available for this automation with the capability to adapt to the size-change and body-deformation. In this research, through the understanding of the anatomy of chicken shoulder joints, a new processing method associated with a simple mechanism is proposed. Note that the scope of this paper is to design a device which has the ability to adapt the bio-material deformation during cutting. The adaptability will be further studied through the motion control and force control.

In the following, the anatomy of the cutting related chicken shoulder is studied and the cutting trajectories are specified in Section II first. According to front halves' transportation methods in a poultry processing plant, the cutting system is specified and the mechanism is then simulated in Sections III and IV. The driven system is then selected and verified in Section V. After the discussion in Section VI, conclusions are drawn in Section VII.

II. Deboning Related Chicken Shoulder Anatomy

A. Chicken Shoulder Anatomy

The shoulder joint deboning task is to sever the connection between the chicken wing and main body, meanwhile the connection between the breast meat and the wings has to be kept in order to facilitate the pulling of the butterfly. The related anatomic structures are the bone structure and the connection between the wing and the carcass. Figure 2 shows the skeleton of a chicken front half. Reference [7] has shown the detailed study, however, their anatomy study cannot be

directly applied to the cutting trajectory identification for the device design.

The shoulder bone girdle is formed by the connection of the scapula, coracoid and clavicle. The two girdles connect to the vertebrate through some ribs. The coracoids connect together through the keel bone. In fresh chickens, the wish bones (clavicles) connect with the keel bone through some soft tissues. Compared with Figure 2, the location and orientation of the humerus and breast meat relative to the skeleton is shown in Figure 3. The area below the breast meat under line *AB* and between coracoid and humerus is the starting potion of the tender meat. The connection between humerus and the carcass includes ligaments, tendons, meat and skin, which form a ball-socket shoulder joint. For fresh front half, when the chicken wing is pulled, a small gap (about 2 -5 mm) is created between the humerus and the shoulder bone girdle. This gap provides the space for a blade to enter the joint. The gap increases when the top ligament which connects the humerus to the carcass is cut.

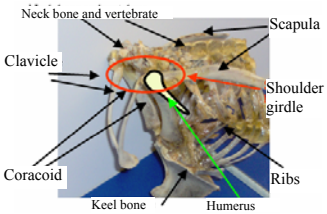

Figure 2: Front half skeleton.

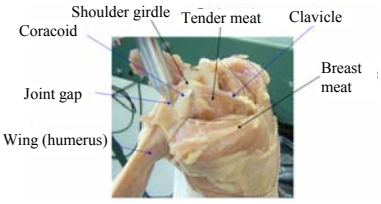

Figure 3: Skeleton and meat positions.

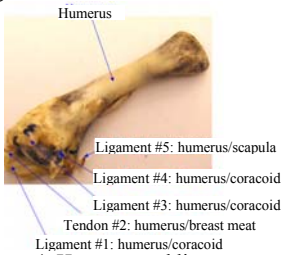

Figure 4: Humerus and ligaments.

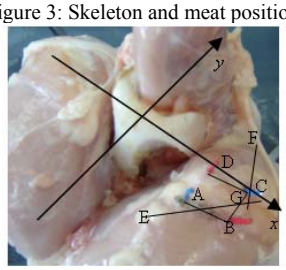

Figure 5: Cutting area top view.

There are 5 main ligaments/tendons connecting the humerus to the carcass as shown in Figure 4. Three of them connect the humerus with the coracoid, one tendon connects the breast meat with the humerus through a hole in the middle of the coracoid and one ligament connects the scapula with the humerus. The structure under *BC* is a thin layer of meat (about 5mm), the gap between the humerus and the coracoid (gap of the ball and socket of the shoulder joint), and the connecting ligaments/tendons. Figure 5 shows the top view of a front half. In order to descript the cutting trajectory, a frame system *oxyz* on the chicken is defined. The upward direction of the cone is the positive direction of the *z* axis. Two points are identified as reference points: in the z direction, the highest coracoid points on the left and right sides. The *x* axis direction is formed by connecting these two points and the positive direction is from left to right. The *y* axis is then defined using the right-hand rule. Point *A* is a point on the clavicle where the clavicle connects to the coracoid; *G* is the middle point of the gap between humerus and coracoid; *BC* is the joint gap location. The locations of lines *AB* and *BC* are the cutting lines.

The "must cut part" (cuts that must be performed in order to safely and efficiently remove the butterfly) under *BC* is shown in Figure 6(a) as the shaded area *BB′C′C* when viewed along the wing direction (Figure 3) and from the wing to the body direction with the wing being removed. Note that the ligaments and tendons occupy about 3/4 of a circle perimeter around the joint and leave about 1/4 joint near the neck empty (dark green arc in Figure 6(a)). The "must cut part" under *AB* is shown in Figure 6(b) when viewed along the positive *y* axis, where the shadow part shows the breast meat under *AB* and the part below *AB′* is the tender meat and keel bone. Note that the dimensions shown in Figure 6 are the average length. They were obtained from the measurement using FARO equipment [8]. For different size chickens, the above dimensions are different. The cutting device should have the ability to adapt to the dimension change.

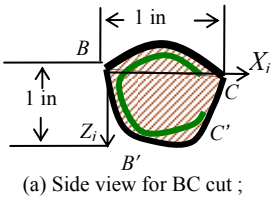

(a) Side view for BC cut ;

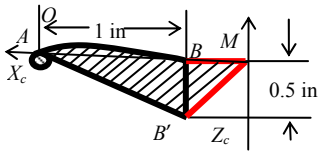

(b) Front view for AB cut;

Figure 6: Front half cutting area identification.

In this paper, the cutting trajectory following *BB′C′C* is called the *joint cut*, and the cutting trajectory following *ABB′M* is called the *clavicle cut*. Additional area must be cut (*MB′B*) in order to account for the entering of the blade into the meat.

B. Cutting Area and Cutting Trajectory

One of the design requirements is that the front half translates at 10in/s, which is the speed of the conveyor in this part of the plant. Based on the average dimension of the front halves, the cutting trajectories are specified in Tables 1 and 2. Note the (X_c, Z_c) and (X_j, Z_j) are the coordinates measured in the frames shown in Figure 6 (a-b), respectively.

Table 1: Clavicle cut trajectory.

Motion	Position (X_c, Z_c) in inch	Time
Origin	(0, 0);	0
Size adaptation motion	(1, 0)	0.5s
Height adjustment motion	(1, 1)	0.2s
Pushing in motion	(1, 1.5)	0.025s
Clavicle cutting motion	(1 ,1)	0.1s
Back to origin	(0, 0)	0.375s
Total time		1.2s

Table 2: Joint cut trajectory.

Motion	Position (X_j, Z_j) in inch	Time
Origin	(0, 0)	0s
Size adaptation motion	(1, 0)	0.2s
Height adjustment motion	(1, 1)	0.2s
Joint Cut motion	(1, 2.8)	0.2s
Back to origin	(0, 0)	0.6s
Total time		1.2s

III. Deboning System and Cutting Device

It is assumed that front halves are fixed on cones and the cones move together with the chain or conveyor. According to the current cone design technology, it is also assumed that the cones can provide all the required roll, yaw and pitch motions. The other requirements for the cutting device are (i) the 'must cut' trajectory must be followed, (ii) the device must adapt to variation in bird size, (iii) cutting force must be small enough such that the cutting cannot damage the carcass and clavicle

and (iv) the deformation is small such that the shoulder joint can be cut by following the desired cutting trajectory.

Considering the procedure to harvest the breast meat, five working stations are applied as shown in Figure 7. The first one is the vision station which is used to identify the location of the bird's joints relative to the cone. The second is the scapula cut station. The next two are for the left and right clavicle cuts. The last one is for the joint cut. The CAD drawing of the prototype is shown in Figure 8.

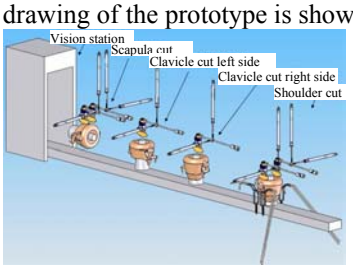

Figure 7: Cutting system diagram

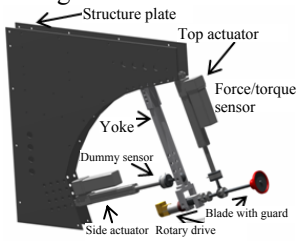

Figure 8: Cutting device

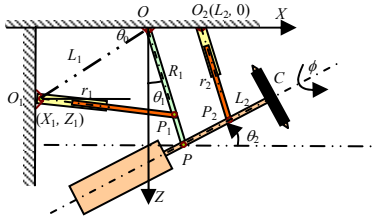

Figure 9: Schematic illustration of the cutting device.

Note the individual cutting device in Figure 7 is driven by a pneumatic system. Its structure was explained in [9]. However, the device in Figure 8 is an electrical driven system. The cutting devices in Figure 7 will be replaced with the cutting device shown in Figure 8 in the real system. Although the pneumatic device can provide enough speed for the cutting motion, the switch from the pneumatic system to electrical system is based on two reasons: (i) it is not fast enough to response to the bone detection and (ii) it cannot satisfy the critical requirement of the cutting accuracy for following the desired trajectory. Also the system in Figure 8 is a two link system and the system in Figure 7 is a one link system. Their kinematics and dynamics are totally different.

The schematic drawing of the cutting device is shown in Figure 9. The cutting tool is basically a 2-link mechanism with links *OP* and *PC*. The handle is driven by the translation motion of two pistons of the two actuators, respectively. Frame *OXZ* is fixed in the space, where *Y* is not shown due to the plane mechanism. Point *O* is a pin joint connected to a space-fixed location and point *P* is also a pin joint. The device has 3 DOFs, rotations around points *O*, *P* and *C*. The driven system includes two electrical actuators, called top actuator and side actuator and one rotary motor. The top actuator, which connects to the handle at point P_2, is mainly for the cutting motion. The side actuator, which connects to the handle at point P_1, is mainly for size adaptation motion. The other side of each linear actuator is fixed to the structure plate through pin joints. The two actuators and the handle can rotate freely relative to the joints.

In the following, subscript 2 expresses the parameters for the top actuator and subscript 1 is for the side actuator. In *OXZ* frame, the notations are as follows: *O* (0, 0) is the origin of the space-fixed frame. O_1 (X_1, Z_1) is the base of the side actuator. O_2 (L_2, 0) is the base of the top actuator. P_1, P_2 are the locations of the linear actuators connecting to the handle, where $OP_1 = R_1$, $OP = R$, $PP_2 = L_2$, $PC = L$, $O_1P_1 = r_1$, $O_2P_2 = r_2$, $OO_1 = L_1$, $\angle ZOP = \theta_1$, and $\angle XPC = \theta_2$. *C* (*x*, *z*) is the center of the rotary blade. ϕ is used to express the rotation of the cutter which is not consider in this paper.

Three sets of DOFs are identified: $\{\Re: q_1 = r_1, q_2 = r_2, q_3 = \phi\}$ or $\{\Theta: q_1 = \theta_1, q_2 = \theta_2, q_3 = \phi\}$ or $\{\Lambda: q_1 = x, q_2 = z, q_3 = \phi\}$, where q_1, q_2, q_3 are generalized coordinate. The initial position of the system is that *OP* is on *OZ*, and $O_2O // PP_2 // O_1P_1$ ($OP // O_2P_2$). The forward kinematics is from $\Re$ to Λ and the inverse kinematics is from Λ to $\Re$.

A. Relationship between Λ and Θ

The relationship between *x*, *z* and θ_1, θ_2 can be obtained as

$$\begin{bmatrix} x \\ z \end{bmatrix} = L\begin{bmatrix} c_2 \\ -s_2 \end{bmatrix} + R\begin{bmatrix} s_1 \\ c_1 \end{bmatrix}, \tag{1}$$

where $s_1 \equiv \sin(\theta_1)$, $c_1 \equiv \cos(\theta_1)$, $s_2 \equiv \sin(\theta_2)$, and $c_2 \equiv \cos(\theta_2)$. By solving θ_1 and θ_2, there are

$$\theta_1 = \sin^{-1}\left(\frac{x^2 + z^2 + R^2 - L^2}{2R\sqrt{x^2 + z^2}}\right) - \sin^{-1}\left(\frac{z}{\sqrt{x^2 + z^2}}\right), \tag{2}$$

$$\theta_2 = \sin^{-1}\left(\frac{x^2 + z^2 + L^2 - R^2}{2L\sqrt{x^2 + z^2}}\right) - \sin^{-1}\left(\frac{x}{\sqrt{x^2 + z^2}}\right). \tag{3}$$

The relationship between the velocity of the center of the rotary blade and the angular velocity of the mechanism is

$$\begin{bmatrix} \dot{x} \\ \dot{z} \end{bmatrix} = \begin{bmatrix} -Ls_2 & Rc_1 \\ -Lc_2\dot{\theta}_2 & -Rs_1 \end{bmatrix}\begin{bmatrix} \dot{\theta}_2 \\ \dot{\theta}_1 \end{bmatrix}, \tag{4}$$

or

$$\begin{bmatrix} \dot{\theta}_2 \\ \dot{\theta}_1 \end{bmatrix} = \begin{bmatrix} -Ls_2 & Rc_1 \\ -Lc_2 & -Rs_1 \end{bmatrix}^{-1}\begin{bmatrix} \dot{x} \\ \dot{z} \end{bmatrix}. \tag{5}$$

B. Relationship between ℜ and Λ

Using the law of Cosine on triangle OO_1P_1, there is

$$r_1^2 = L_1^2 + R_1^2 + 2L_1R_1\sin(\theta_1 - \theta_0). \tag{6}$$

Thus

$$\dot{r}_1 = L_1R_1\cos(\theta_1 - \theta_0)\dot{\theta}_1 / r_1. \tag{7}$$

The vectors $\mathbf{r}_{OP_2}$ and $\mathbf{r}_2$ can be expressed as

$$\mathbf{r}_{OP_2} = \begin{bmatrix} Rs_1 + L_2c_2 & 0 & Rc_1 - L_2s_2 \end{bmatrix}^T,$$

$$\mathbf{r}_2 = \begin{bmatrix} Rs_1 + L_2c_2 - L_2 & 0 & Rc_1 - L_2s_2 \end{bmatrix}^T,$$

thus

$$r_2^2 = (Rs_1 + L_2c_2 - L_2)^2 + (Rc_1 - L_2s_2)^2. \tag{8}$$

There is

$$r_2\dot{r}_2 = (Rs_1 + L_2c_2 - L_2)(Rc_1\dot{\theta}_1 - L_2s_2\dot{\theta}_2) + (Rc_1 - L_2s_2)(-Rs_1\dot{\theta}_1 - L_2c_2\dot{\theta}_2).$$

So

$$\dot{r}_2 = \frac{1}{r_2}\begin{bmatrix} (Rs_1 + L_2c_2 - L_2)Rc_1 - (Rc_1 - L_2s_2)Rs_1 \\ -(Rs_1 + L_2c_2 - L_2)L_2s_2 - (Rc_1 - L_2s_2)L_2c_2 \end{bmatrix}^T\begin{bmatrix} \dot{\theta}_1 \\ \dot{\theta}_2 \end{bmatrix}, \tag{9}$$

and

$$\dot{\theta}_2 = \frac{r_2\dot{r}_2 - (Rs_1 + L_2c_2 - L_2)Rc_1 - (Rc_1 - L_2s_2)Rs_1\dot{\theta}_1}{(Rs_1 + L_2c_2 - L_2)L_2s_2 - (Rc_1 - L_2s_2)L_2c_2}. \tag{10}$$

From the above relationships, both the direct kinematics and inverse kinematics can be formulated.

IV. System Dynamic Model Construction

A. Desired Trajectory

The length of each link used on the desired trajectory generation is listed in Table 3.

Table 3: System physical parameters (unit is inch).

R_1	R	L_2	L	L_1
11.9	14.9	5	11	19.07

By shifting the cutting trajectories shown in Table 1 and Table 2 with L distance from the x coordinate and R distance from the z coordinate, the desired cutting trajectories can be generated. For the clavicle cut, the desired trajectory of the center of the rotary blade in OXZ frame is shown in Figure 10. For the joint cut, the desired trajectory of point C in OXZ frame is shown in Figure 11. Note that the requirements for the generation of the desired trajectories are as follows: (i) the speeds at starting point and the ending point of each trajectory segment are zero and (ii) the acceleration is a constant during accelerate and decelerate period. The two requirements ensured the smoothness of the generated trajectories.

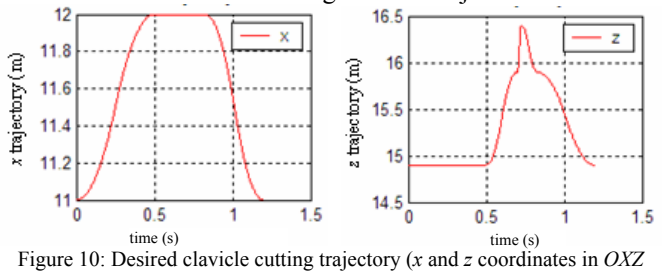

Figure 10: Desired clavicle cutting trajectory (x and z coordinates in OXZ frame).

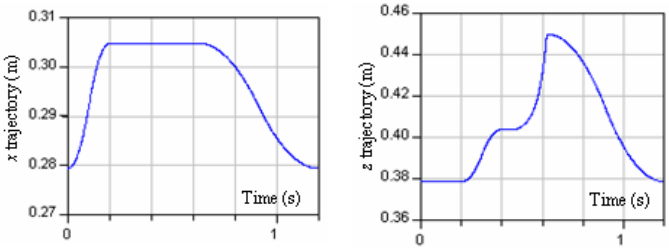

Figure 11: Desired joint cutting trajectory (x and z coordinates in OXZ frame).

B. Dynamic Model Construction

Based on the desired trajectory and the kinematics shown in Section III, the desired motor rotation angles and actuator translation distances can be calculated. The desired angles serve as the desired input for motor control.

The rotary motion of the motor was translated to the linear motion of the actuator piston using a ball-screw system. Thus a model for the ball–screw mechanism was needed for the translation from the torque / angular velocity of the rotary motor to the force / linear speed of the linear actuator. There are many techniques for modeling of a ball-screw system, such as [11] and [12]. The method used in this research was different from the available literature because some of the parameters used in the literature were not physically available from the manufactures. By using the manufacture provided experimental data, the method used in this paper is to build a point-by point mapping function between the input torque/angular speed and force/linear speed. The RSM12 SN02 ball-screw from Tol-O-Matic Inc. [13] is used as an example to explain this method. Figure 12 shows relationship between the torque/speed and force/speed from actual measurements provided by the manufacture, where the value at point K_1 in Figure 12 (a) is transferred to the value at point K_2 in Figure 12 (b) and the red line in Figure 12 (a) is transferred to the red line in Figure 12 (b). Thus a scale factor is used to map all the points in Figure 12 (a) to Figure 12 (b). Note that the speed mapping is just related to the "inch per turn" parameters in the catalog [13]. Some of the mapping results were shown in Figure 13. Although this mapping method considers the ball-screw system as a black box, the internal friction, backlash, kinematics and dynamics were all considered in the model

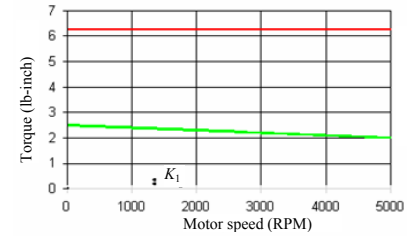

(a) Torque- speed relationship,

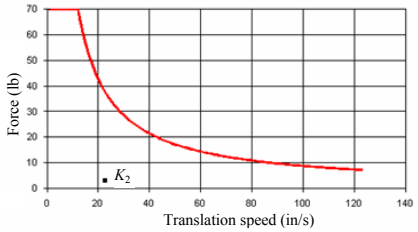

(b) force- speed relationship.

Figure 12: Manufacture-provided graphical relationship between torque / angular speed and force / linear speed.

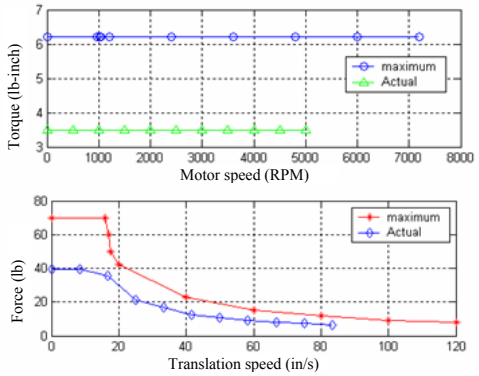

Figure 13: Results of mapping from torque speed relationship to force speed relationship.

The dynamic model using the Dymola [10] software has been constructed and simulation results were obtained. The model is not shown in this paper. The basic functions of the dynamic model are (i) realization of the kinematics by converting the desired x, z trajectory to two motor rotation angles as the commands for motor position control, (ii) realization of the ball-screw model, (iii) motor function realization by using the models given by Ogata [14] with speed and torque constraints, (iv) motor motion control

realization and (v) the dynamic mechanism realization, including the models of the pin joints, links with mass and inertial, gravity, world coordinate reference system, passive rotation joints, active rotation joints and the external forces changing with time. The mass and inertia of the proposed system used in the model are listed in Table 4 and the selected motor for linear motion is MRV11 [13] and its parameters are shown in

Table 5.

Table 4: Mass and inertia of the proposed system.

Components	mass (kg)	Mass center position (m)	Inertia (kg-m^2)
Rotary motor, second link (PC) and blade	0.61	(0, -0.002219, -0.006975)	$\begin{bmatrix} 0.004287 & 0 & 0 \\ 0 & 0.004258 & 8.99e-5 \\ 0 & 8.99e-5 & 0.0001113 \end{bmatrix}$
Linear motor only	1.51 (2 items)	(1.2227e-5, 0.02182, -0.09843)	$\begin{bmatrix} 0.02105 & 0 & 0 \\ 0 & 0.01965 & -2.8e-3 \\ 0 & -2.8e-3 & 0.001796 \end{bmatrix}$
Linear motor shaft and ball-screw system	0.36 (2 items)	(0, -1.3e-5, -0.2942)	$\begin{bmatrix} 0.03302 & 0 & -4.5e-8 \\ 0 & 0.03302 & 1.4e-6 \\ -4.5e-8 & 1.4e-6 & 3.252e-5 \end{bmatrix}$
Link (from O to P_1)	0.60	(0, -0.1387, 0)	$\begin{bmatrix} 0.01638 & 0 & 0 \\ 0 & 1.8e-4 & 0 \\ 0 & 0 & 0.01652 \end{bmatrix}$
Link (from P_1 to P)	0.14	(0, -0.03962, 0)	$\begin{bmatrix} 2.8e-4 & 0 & 0 \\ 0 & 1.3e-4 & 0 \\ 0 & 0 & 4e-4 \end{bmatrix}$
Total	5.09		

Table 5: Motor parameters.

Back EMF constant	Torque constant	Motor inductance	Motor resistant	Motor inertia	Maximum speed
6.06 v/1000rpm	0.1N-m/amp	1.63 mH	2.24Ω	5.72 e-6 kg-m^2	5000rpm

V. Simulation Results

A. Joint Cut

In joint cut, the center of the blade (Point C) should follow the trajectory shown in Figure 11. Thus by specifying the x and z coordinates of point C, the angles θ_1 and θ_2 can be calculated using (2) and (3). The strokes for each axis can then be computed using (6) and (8). Based on the ball–screw torque-force transformation relationship shown in Figure 12, the linear distance (6) and (8) are converted to the motors' rotation angles. The obtained motor rotation angles were obtained and shown as the blue lines in Figure 14 and Figure 15 for the side and top motors, respectively. By tuning the parameters of the applied PID controllers, the outputs of the side and top motors' rotation angles were obtained and shown as the red lines in Figure 14 and Figure 15, respectively. It can be noticed that the red lines covered the blue lines which means that the desired rotation angles were followed well by the motor actual rotation angles.

The desired x and z coordinates were shown in Figure 16 as the red lines. Using the 'sensor' function in Dymola, the coordinates of point C in the world frame system were also measured and shown in Figure 16. It can be seen that point C coordinates were fully realized by the system. This proved the kinematics formulation in Section III and the proposed motor systems could achieve the motion requirements.

This dynamic model also provided the results of the actuator strokes (Figure 17) and the motor torques (Figure 18). It is noticed that the desired trajectories of the two actuators were followed well by the actual moving distance. Although big vibrations happened in the motor torque, the output trajectory was stable and followed the input trajectory well.

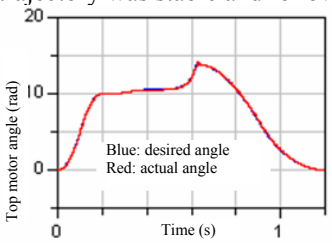

Figure 14: Desired and actual side motor rotation angles.

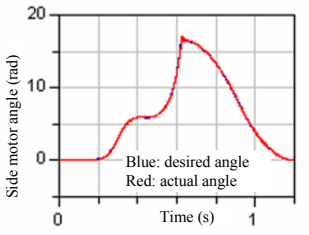

Figure 15: Desired and actual top motor rotation angles.

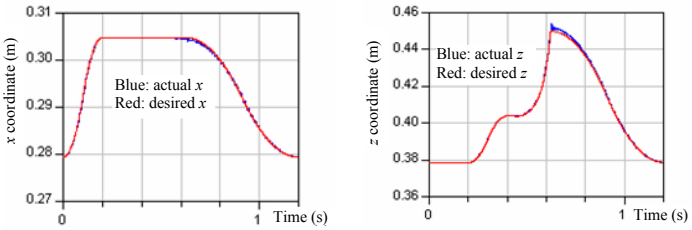

Figure 16: Desired and actual cutting trajectory: x (left), z (right).

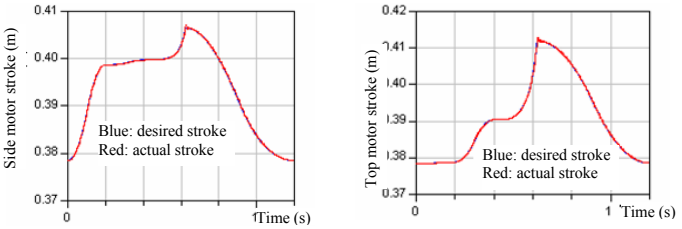

Figure 17: Desired and actual linear moving distance: side (left), top (right).

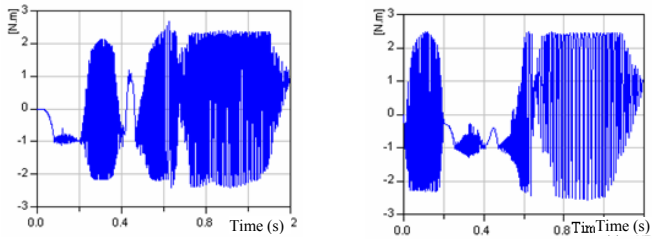

Figure 18: Actual torque from side motor (left) and top motor (right).

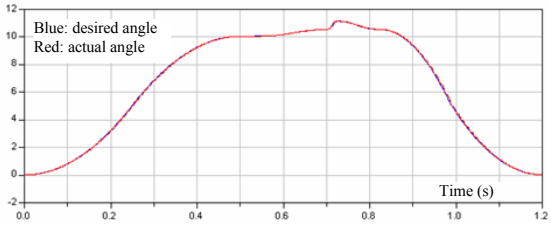

Figure 19: Desired and actual side motor rotation angles.

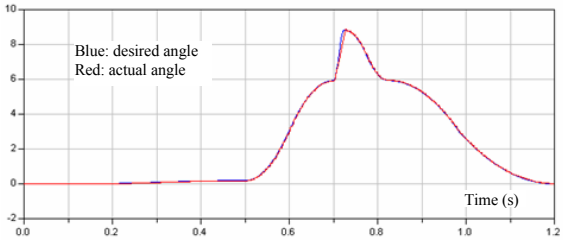

Figure 20: Desired and actual top motor rotation angles.

B. Clavicle Cut

In clavicle cut, the desired trajectory shown in Figure 10 is used. The same model in Section V (A) was used. By tuning the control gains, the obtained results were similar to those

obtained in joint cut. The desired (in blue) and the actual (in red) rotation angles of the side motor were shown in Figure 19 and the desired (in blue) and the actual (in red) rotation angles of the top motor were shown in Figure 20. It can be seen that the desired trajectories were followed well.

The strokes of the two linear actuators are shown in Figure 21. In order to generate the clavicle cut motion, the torques provided by the side and top motors are shown in Figure 22, respectively. It can be seen that the motor can generate the required motion.

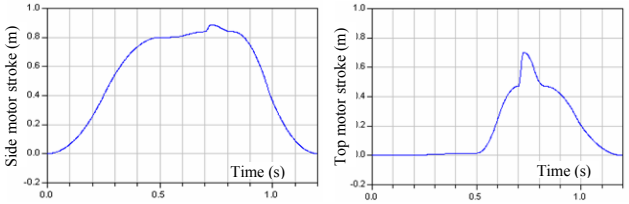

Figure 21: Stroke of the two linear motors.

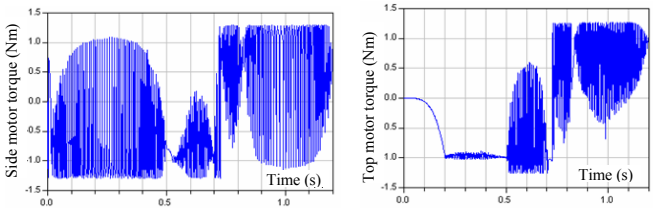

Figure 22: Actual torque from side motor (left) and top motor (right).

VI. Discussion

For the clavicle cut, the critical requirements are (i) to cut through the breast meat, (ii) to cut fully to the clavicle bone, (iii) to avoid cutting too much of the breast meat and (iv) to avoid breaking the clavicle bone. Normally, the thickness of the breast meat on the clavicle cutting path is about 1/4 inch. In the design, 1/2 inch cutting distance is provided to make sure the breast meat can be fully cut. By selecting electrical linear actuators, the response time of the cutting device is fast enough to avoid cutting through the clavicle.

For the joint cut, the critical requirements are (i) to cut through the joint, (ii) to avoid cutting too much of the breast meat and (iii) to avoid cutting into either the humerus or the coracoid. The depth of the joint is normally about 1 inch. In the proposed design, sufficient stroke is provided to ensure the cutting depth of the joint. In order to avoid cutting into the bones, the joint location information from the camera station and the knife orientation are very important. Further algorithms will be developed to solve the problem when bones are cut based on the force/torque sensor feedback. These control algorithms are to be integrated with the models for cutting of bio-material [15]. This will provide the theoretical basis for all of the control system development.

VII. Conclusions

In order to overcome the difficulties in the automation of the poultry deboning due to the natural variability of birds' size and deformable bodies, in this research, a new deboning system and a cutting device have been proposed. The following conclusions were drawn: (i) The deboning related chicken shoulder anatomy was described. The simple cutting trajectories were identified in order to realize both easy deboning and chicken size adaptation with good yield. (ii) The kinematics of the cutting device was formulated and a full dynamic model of the cutting device was realized. By comparing with the measured actual cutting trajectory in the dynamic model, the kinematics was verified. (iii) The results from the dynamic simulation shown that the selected driving system was capable to provide the required torques, to follow the desired trajectories and to provide the fast response for bone detection. By providing the extra moving distance, the system has the ability to adapt to the dimension change. The force/torque sensor in the device will provide the capability for force control to realize intelligent cutting. A functional prototype of this device has been built currently. The size adaptation control and bone detection algorithm will be further studied in this research based on the prototype.

Acknowledgement

This project is supported by the State of Georgia through the Agriculture Technology Research Program at the Georgia Tech Research Institute.

References

[1] Stork Gamco, Inc. (2007 Jan.), Available: *http://stork.com/gamco /page.html?id =7610*.

[2] Meyn Food Processing Technology, (2007 Jan.), Available: *http://www. meyn.nl/index.php?option=com_content&task=view&id=123&Itemid= 34*.

[3] W. Daley, T. He, K-M Lee and M. Sandlin, "Modeling of the natural product deboning process using biological and human models," in the *Proceedings of 1999 IEEE/ASME International Conference on Advanced Intelligent Mechatronics*, 19-23 Sept. , 1999, pp. 49 – 54.

[4] B. Heck, "Automated chicken processing: machine vision and water-jet cutting for optimized performance," *IEEE Control Systems Magazine*, 26(3), June, 2006, pp. 17-19.

[5] P. G. Dempsey and R. W. McGorry, "Investigation of a pork shoulder deboning operation," *Journal of Occupational and Environmental Hygiene*, vol 1, 2004, pp. 167-172.

[6] R. W. McGorry, P. C. Dowd and P. G. Dempsey, "The effect of blade finish and blade edge angle on forces used in meat cutting operations," *Applied Ergonomics,* Elsevier publications, vol. 35, 2005, pp. 71-77.

[7] F. Chamberlain, *Atlas of Avian Anatomy*. Michigan State College, Agricultural Experiment Station, East Lansing, MI. Hallenbeck Printing Company, Lansing, MI, 1943.

[8] FARO Technologies Inc., (2007 Jan.), Available: *http://www.faro.com/content.aspx?t=us&co nten =pro&item=1*.

[9] D. Zhou, J. Holmes, W. Holcombe, K-M Lee and G. McMurray, "Automation of Bird Front Half Deboning Procedure: Design and Analysis," accepted for publication in *the 12th IFToMM World Congress*, Besançon (France), 18-21, June 2007.

[10] Dynamic Modeling Laboratory, (2007 Jan.), Available: *http://www. dymola.com /index.htm*.

[11] C. C. Wei and J. F. Lin, "Kinematic Analysis of the Ball Screw Mechanism Considering Variable Contact Angles and Elastic Deformations," *Journal of Mechanical Design*, 125(4), 2003, pp. 717-733.

[12] K. R. Eldredge and D. Tabor, "The Mechanism of Rolling Friction. I. The Plastic Range" in the *Proceedings of the Royal Society of London. Series A, Mathematical and Physical Sciences*, Vol. 229, No. 1177, 1995, pp. 181-198.

[13] Tol-O-Matic, *Axi-dyne MRV Brushless Servo Motors*, PDF file, (2007 Jan.), Available: http://www.tolomatic.com /products/index.cfm.

[14] Ogata K., *Modern control engineering*, 3rd edition, Upper Saddle River, N.J., Prentice Hall, 1997.

[15] D. Zhou , M. Claffee K-M Lee and G. McMurray, "Cutting, 'by Pressing and Slicing', Applied to the Robotic Cut of Bio-materials, Part II: Force during Slicing and Pressing Cuts" , in the *Proceedings of the 2006 IEEE International Conference on Robotics and Automation (ICRA06)*, Orlando, FL, May 15-19, 2006, pp. 2256-2261.